International Journal of Thin Films Science and Technology

http://dx.doi.org/10.18576/ijtfst/050206

Synthesis of GaN Thin Film Using a Low-Cost Electrochemical Deposition Technique for Hydrogen Gas Sensing

K. Al-Heuseen[*]

Ajloun University College, Al-Balqa Applied University, Jordan.

Received: 21 Mar 2016, Revised: 2 Apr. 2016, Accepted: 10 Apr. 2016.
Published online: 1 May 2016.

Abstract: GaN thin films were synthesized on n-Si (111) and n-Si (100) substrates using a low-cost electrochemical deposition technique for hydrogen gas sensing. SEM images revealed that the grown GaN films consist of a network of nanoflake structures. XRD analyses showed both the hexagonal wurtzite and the cubic zinc blend GaN phases for the deposited films with the crystallite size around 18-19 nm. Photoluminescence spectrum showed that the energy gaps of h-GaN and c-GaN were near 3.39eV and 3.2eV respectively at 300K. Corresponding I-V characteristics of the Schottky diodes were recorded before and after hydrogen gas exposure. Thermionic emission model was used to analyses I-V data. The barrier height increased significantly with hydrogen flow rate. Sensitivity and response time were discussed for the two samples.

Keywords: Electrochemical deposition; Hydrogen gas sensor; Schottky diode; low cost.

1 Introduction

Hydrogen gas has a wide range of applications in modern life and it is gaining more interest as an alternative fuel. Therefore, the development of hydrogen gas sensors has become a necessity for leak detection purposes in many applications such as hydrogen fueled automobiles and spacecraft and to monitor hydrogen emission in many industrial applications since hydrogen is a hazardous, odorless, and highly flammable gas [1-4]. Due the nature of applications in fuel cells, sensors that are capable in operating at high temperature and corrosive ambient are highly desirable.

GaN is an ideal material for such kinds of applications, due to its wide-band gap and thermal stability. The material is also chemically stable, with the only known wet etchant being molten NaOH or KOH, making it very suitable for operation in chemically harsh environments or in radiation fluxes. In addition, GaN gas sensors have the unique advantage of integration with GaN-based solar-blind UV photodetector or high power, high temperature electronics units on the same chip. Commonly, GaN is crystallized in a thermodynamically stable hexagonal (wurtzite) structure. However, the hexagonal GaN (h-GaN) always contains strong piezoelectric and spontaneous polarization fields that would limit the performance of optoelectronic devices. The metastable cubic-phase GaN, which has a zinc-blende structure does not exist in nature.

Growing GaN in cubic structure is a possible way to eliminate the internal fields and it can be fabricated on a crystalline substrate with a cubic structure like Si(100). In addition, cubic GaN offers easy cleavage along (100) facet orientation, and it has a high carrier mobility especially holes due to higher crystal symmetry.

However, preparing h-GaN and c-GaN is still high cost and needs special conditions using various conventional growth techniques, including metalorganic chemical vapor deposition (MOCVD) [5], reactive molecular beam epitaxy (MBE) [6], hydride vapour phase epitaxy (HVPE) [7] and reactive sputtering [8]. There are numerous reports on synthesis of GaN powders by chemical reaction [9, 10], however, using this method to synthesis GaN thin films is still a challenge. On the other hand, electrochemical deposition (ECD) is very promising method to grow GaN films due to the following advantages: the thickness and surface morphology can be easily controlled as well as the amount and type of doping by growth parameters, the deposition rate is relatively high, the experimental setup is low-cost, and it does not require a high temperature, which reduces the thermal mismatching between GaN and substrate and this enhances the sensitivity of gas sensing [11-13]. Despite of that, there are very few reports on using ECD in making GaN thin films [14-16] and to the best of

[*]Corresponding author E-mail: kalhussen@yahoo.com

© 2016 NSP
Natural Sciences Publishing Cor.

our knowledge, there are no reports on using this method to synthesis GaN thin film for hydrogen gas sensing.

For hydrogen detection Pd or Pt are the metals most often used in Schottky-type sensors [17,18]. This motivate our study to use other metal like Ni. In this work Ni is used because it has a work function of 5.15 eV, and it could form a good Schottky contact with n-GaN. In addition, Ni is more chemically active and provides better adhesions to the samples. In this work, we report the hydrogen-sensing properties of Schottky diodes (Ni/GaN/Ni) made out of GaN thin films grown by ECD on n-Si (111) and n-Si (100) substrates at 20ºC using constant current density. We found that the sensitivity of the diode is affected by the flow rate of hydrogen and the microstructure of the Ni.

2 Experimental Procedure

GaN thin films were grown by electrochemical technique using an aqueous solution that is prepared by mixing gallium nitrate (Ga $(NO_3)_3$) with ammonium nitrate (NH_4NO_3) in a ratio of (1:1) in deionized water and kept at 20ºC since Ga metals melts at 29ºC [14-16]. N-type Si (111) and Si (100) were used as substrates. Before deposition, Si was cut into 1cm x 1cm substrates. To remove the oxide layer the substrates were cleaned in three solutions; beginning with 50:10:10 $H_2O/NH_4OH/H_2O_2$ for 10 min, then in 1:50 HF: H_2O for 10 min, finally in 60:10:10 $H_2O/HCl/H_2O_2$ at temperature of 80º C for 10 min. Between the cleaning steps, the samples were rinsed with de-ionized water. For deposition, a simple homemade Teflon cell with two electrodes was used. A gallium plate with (99.999 %) purity was used as an anode and Si as a cathode. The distance between anode and cathode was about 0.5 cm. GaN thin films were synthesized using electrochemical deposition under direct current density of 2.5 mA/cm^2 for 12 hours.

After that, Ni Schottky contacts were deposited onto apportion of the sample using thermal evaporation at a base pressure of 3.4x10^{-5}Torr to form a metal-semiconductor-metal (MSM) diode. The interdigitated Ni contacts formed Schottky barriers. The width of each finger is 230 µm and the finger spacing is 400 µm as seen in Fig.1. The experiment was carried inside a sealed chamber with in and out opening. Five different flow rates of 2% H_2 in N_2 gas were used in the experiment starting from 30 to 150 sccm. The test fixture was placed into the chamber with wires connected from the probes to Keithley (model 2400) for measuring the current-voltage (I-V) characteristics of the sample. Fig. 2 shows the schematic diagram of the experimental set up of hydrogen gas sensor.

All deposited films used in this work were characterized before depositing the Ni contracts using various techniques, namely X-ray diffraction (XRD), scanning electron microscopy (SEM), EDX, Raman scattering and photoluminescence (PL) spectroscopy. All experiments in this work were carried out under atmospheric pressure and at room temperature.

High resolution XRD (PANalyticalX'pert Pro MRD) with a Cu-Kα_1 radiation source (λ = 1.5406 Å) was used to assess the crystalline quality, and the lattice parameters of the samples can also be determined from the peak position. Under high resolution measurements, this system has a resolution of 12 arcsec. An integrated SEM (JOEL JSM-6460LV) and EDX (Oxford instruments Analytical Ltd.) system was utilized to analyze the surface morphologies of the samples. For SEM characterization the measurements are performed at 10 kV to measure the surface morphology of the samples. For EDX analyses, measurements are performed at an acceleration voltage of 10 kV and at two different areas of 10m x 6m

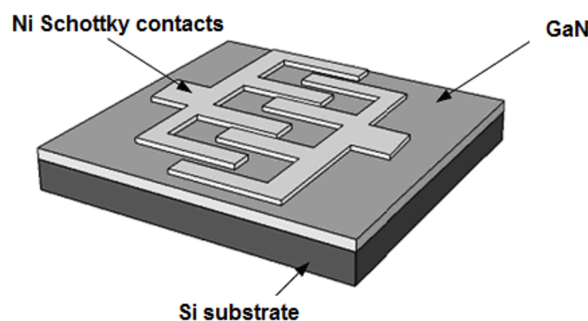

Fig.1. Schematic diagram of the device.

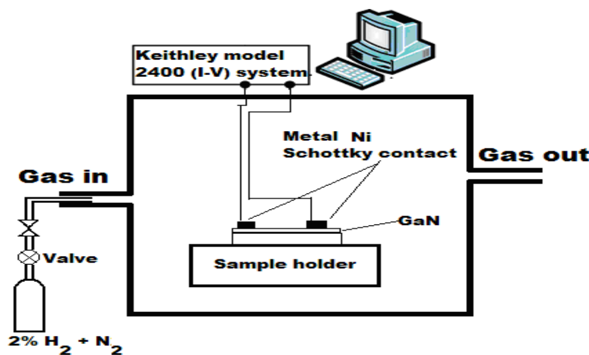

Fig. 2. The schematic diagram of hydrogen gas sensing system.

PL and Raman measurements were performed by using Jobin Yvon HR800UV spectrometer system, that is an integrated confocal micro Photoluminescence and Raman spectrometer. A helium cadmium (He-Cd) laser (325 nm) and an argon ion laser (514.5 nm) were used as an excitation source for PL and Raman measurements, respectively. The penetration depth for He-Cd laser and argon ion laser on GaN were reported to be 1-2 µm and 0.5µm, respectively. For both measurements, the incident laser power was 20 mW. The grating and the hole size were commonly set as 1800 grove/mm and 50 µm, respectively. The Raman scattering experiments were

© 2016 NSP
Natural Sciences Publishing Cor.

carried out in the $z(x,\text{unpolarized})\bar{z}$ scattering configuration. The resolutions of this system for PL and Raman measurements are 0.1 nm and 1 cm^{-1}, respectively.

3 Results and Discussions

Table 1: The percentage of weight and atomic for all elements in the films from EDX data.

Element	GaN/Si(111)		GaN/Si(100)	
	Weight%	Atomic%	Weight%	Atomic%
N	18.09	33.76	10.27	27.49
Ga	42.44	45.15	42.34	34.49
O	11.75	12.25	13.88	23.11
Si	27.71	8.85	33.51	14.91

Fig.3 (a) and (b) show SEM images and corresponding EDX spectrum of GaN thin films deposited on Si (111) and Si (100), respectively. The films were deposited using constant current density of 2.5 mA/cm^2 for about 12 h. The surface morphology of the GaN thin films shows a network of nanoflake structures. As shown in the figure, flakes are described to be a mixture of small and large structures ranging from 100 nm up to one micron. The flakes on the Si (111) sample seem smaller, denser, and more uniform compared to the Si (100) sample. The EDX analyses shows the presence of GaN and Ga_2O_3 for the two samples, the percentage of weight and atomic are included in table 1.

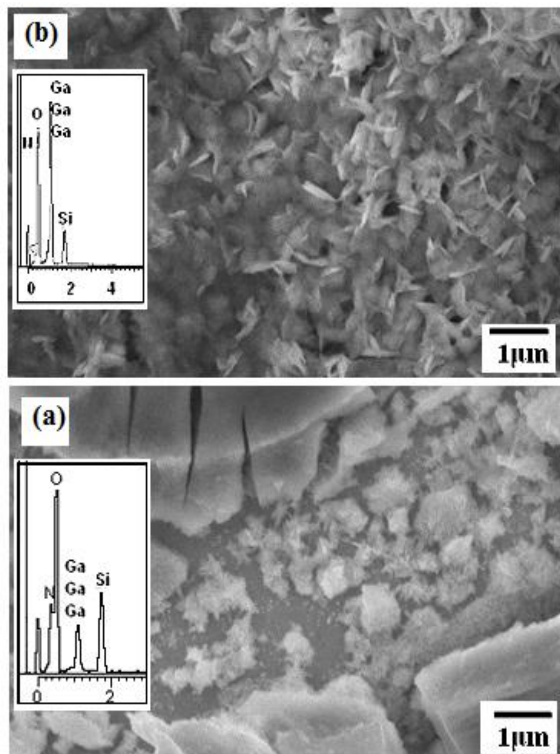

Fig.3. SEM pictures and EDX spectrum of GaN thin films deposited by constant current density 2.5 mA/cm^2 for 12h on (a) Si (111) and (b) Si (100).

Fig. 4 (a) and (b) show typical XRD pattern of GaN films deposited on Si (111) and Si (100) by ECD technique at current density 2.5mA/cm^2, respectively. The XRD spectrum revealed two peaks; one at $2\theta = 32.9^o$ and the other at $2\theta = 40.1^o$ for c-GaN corresponding to reflections from (100) and (002) planes respectively on Si (111) and one peak at $2\theta = 40.1^o$ for c-GaN on Si (100). Another two small peaks at $2\theta = 34.5^o$ and $2\theta = 36.1^o$ for h-GaN corresponding to reflections from (0002) and (1-101) planes respectively on Si (111) and one peak at $2\theta = 34.5^o$ for h-GaN corresponding to reflections from (0002) on Si (100) [19]. A peak with weak intensity of β-Ga_2O_3 could be observed at $2\theta = 37.6\ ^o$ corresponding to reflection plane (11-3) on the two samples. There are four other strong peaks at $2\theta = 28.4^o$ and $2\theta = 58.8^o$ corresponding to Si (111) and Si (222) respectively and at $2\theta = 32.9^o$ and $2\theta = 69.3^o$ corresponding to Si (200) and Si (400) respectively. Thus, the films deposited here contain both the hexagonal and cubic phases of GaN. From the XRD data, the lattice constants have been determined to be a = 3.35 Å, and c = 5.159 Å for hexagonal, which are in a good agreement with reported values [20, 21]. The average size of h-GaN crystals D can be calculated from Scherrer formula:

$$D = \frac{k\lambda}{\beta \cos\theta}$$

Where k is a constant equals to 0.9, λ is the incident x-ray wave and β is given by $\beta = \pi/2$ [FHWM * π/180]. From the calculations, we found that the values of D are between 18 and 19 nm [22].

Fig. 5 shows the PL spectrum of GaN thin films on Si (111) and Si (100) at room temperature. Four peaks at 3.39, 3.2, 3.1 and 1.9 eV can be observed on the PL spectrum of Si (111) while 1.9 eV did not appear on Si (100). The peak positions at 3.39 and 3.2 eV correspond to the band gap for h-GaN and c-GaN respectively, and these values are in good agreement with some reported works [23-26]. The third peak centered at 3.1 eV, may correspond to the donor acceptor (DA) transition [27]. The last observed peak centered at 1.9 eV has low intensity and may be associated

© 2016 NSP
Natural Sciences Publishing Cor.

with the deep level states due to gallium or nitrogen vacancy [28].

A room temperature micro-Raman spectrum of GaN deposited on Si (111) and Si (100) is shown in fig. 6. A strong band is observed at 522.04 cm^{-1}, which is the contribution of the Si substrate, and a small band at 250cm^{-1}, may be due to the acoustic phonons of Si. Three Raman active optical phonons have been clearly assigned to GaN, at 733 cm^{-1} due to A_1 (LO) modes, and two modes for at 140 cm^{-1} and 566cm^{-1} due to E_2 (Low) and E_2 (high) respectively [29].

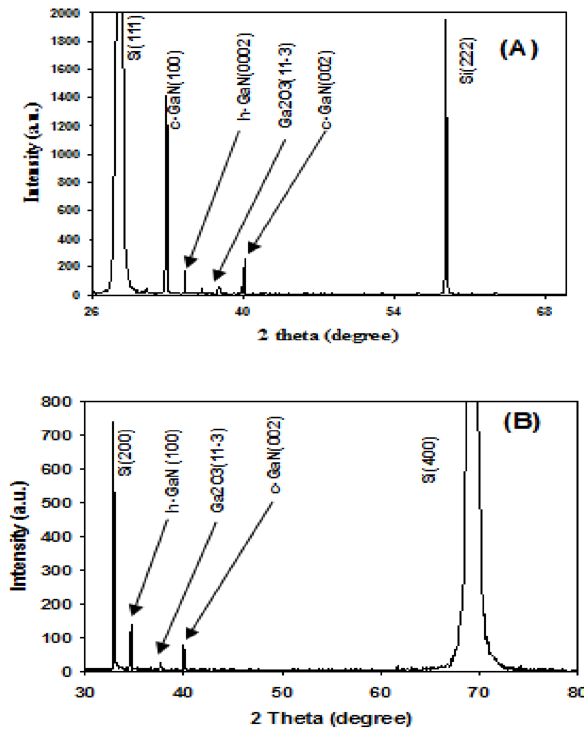

Fig. 4. XRD of deposited GaN films on (A) Si (111) and (B) Si (100) using constant current density of 2.5 mA/cm^2.

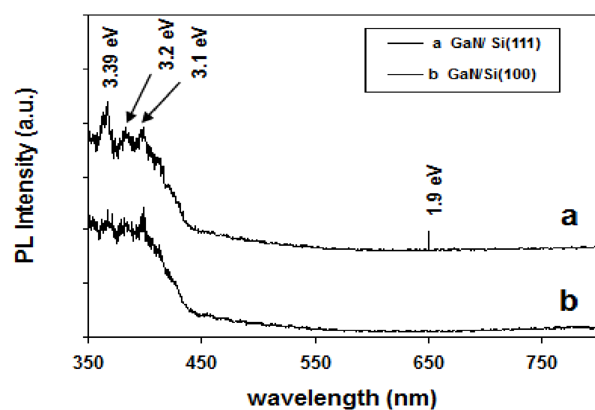

Fig. 5. PL spectra of deposited GaN films for 12h using constant current density 2.5 mA/cm^2 on (a) Si (111) and (b) Si (100).

The current-voltage (*I-V*) plots measured at room temperature for a representative Ni/GaN/Ni Schottky diode on Si (111) and Si (100) after being exposed to different hydrogen flow rates are shown in figure 7 (A) and (B), respectively.

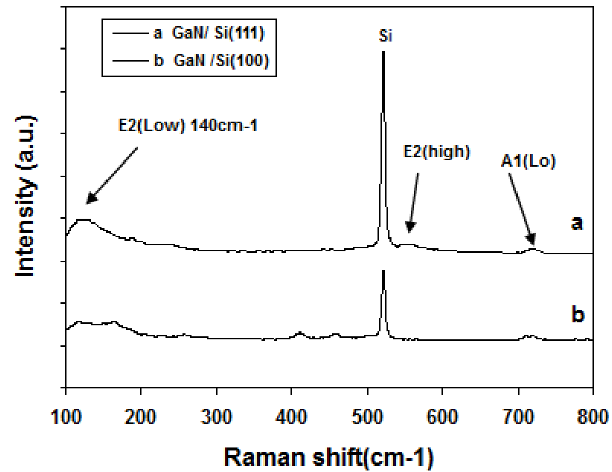

Fig. 6. Raman spectra of GaN deposited for 12h and current density 2.5 mA/cm^2 on (a) Si (111) and (b) Si (100).

From I-V curves, we observed a reduction of current as hydrogen flow rate increased for both samples. The reduction of the current in the presence of hydrogen may be due to an increase in the barrier height between the Ni/GaN interface after H_2 adsorption, and due to lowering of the conductivity. The lowering of conductivity may be a result of the interaction between hydrogen ions and oxygen coming from Ga_2O_3 on the GaN surface.

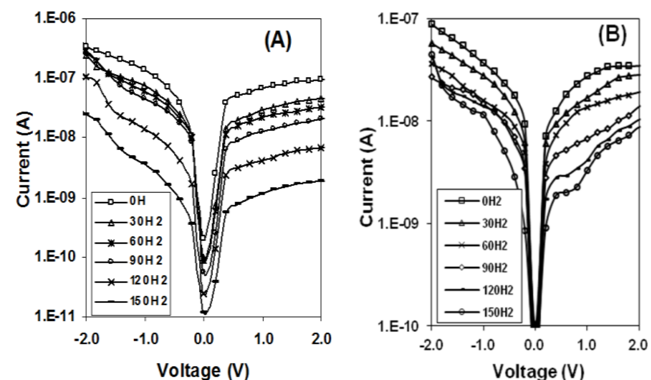

Fig. 7. (I-V) curves of Ni/GaN/Ni gas sensors measured at room temperature for different hydrogen flow rates (A) GaN/Si (111) and (B) GaN/Si (100).

© 2016 NSP
Natural Sciences Publishing Cor.

The adsorbed hydrogen atoms H_2, introduce dipoles at the Ni/GaN interface, whereby an induced voltage ΔV, across the dipoles will cause an increase in the barrier height at the interface [30]. As a result, fewer electrons will be able to exceed the interface barrier height and result in reduced conduction current. A schematic of the change in the barrier height after exposure to H_2 using energy band diagrams is shown in Fig 8.

The forward I-V characteristics of electron transport in metal-semiconductor contacts were analyzed using standard thermionic emission relation [31,32].

$$I_d = I_0 \exp\left(\frac{qV_d}{nkT}\right)\left[1-\exp\left(\frac{-qV_d}{kT}\right)\right] \quad (1)$$

Where V_d is the voltage across the diode, n the ideality factor,k is Boltzman constant, and I_o is the saturation current given by

$$I_0 = AA^{**}T^2 \exp\left[\frac{-q\varphi_b}{kT}\right] \quad (2)$$

Where q is the electron charge T is the temperature A is the contact area A^{**} is the effective Richardson constant and φ_b is the Schottky barrier height. The theoretical value of A^{**} is 26.4 A cm^{-2}K^{-2} based on the effective mass ($m^* = 0.22m_e$) of n-GaN and ($A^{**} = 4\pi q\, m^*k^2/h^3$).

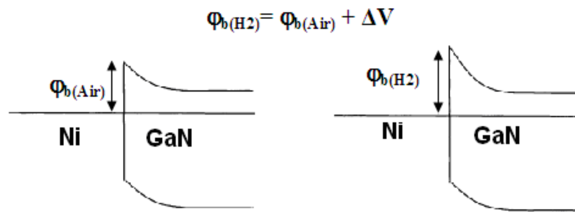

Fig. 8. Schematic diagram of energy band diagrams showing changes in barrier height before and after exposure to H_2 [28].

The barrier height was seen to increase linearly with hydrogen flow rate (see fig. **9(a)**) for both samples. This increase in the barrier height is proportional to the hydrogen flow rate and it also causes the reduction in the measured current after the device has been exposed to H_2.

In addition, these results show that the GaN on Si (111) has a higher barrier height for hydrogen compared to GaN on Si (100). It was also observed that the ideality factor for the two Schottky diodes increased with flow rate of hydrogen (Fig. 9 (b)). The value of n was higher for GaN deposited on Si (111) than n for GaN deposited on Si (100). This may be due to the existence of a large number of surface states related to the nanolayers constituting the diodes.

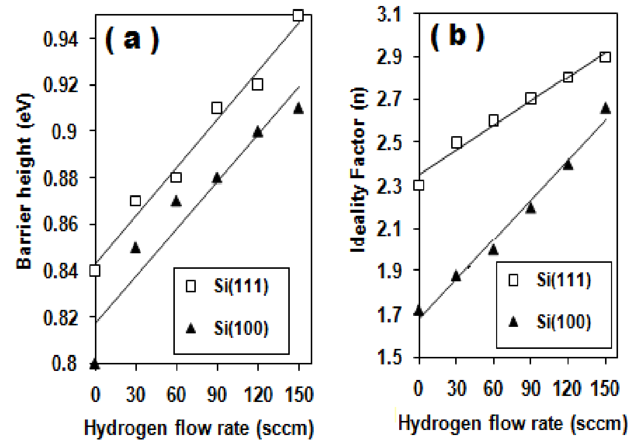

Fig. 9. Variation of (a) barrier potential (φ_b) and (b) ideality factor (n), with different H_2 flow rate for MSM gas sensors of Ni/ECD GaN Schottky diode on Si (111) and Si (100).

For more analyses Fig. 10 shows the consecutive current responses of both devices with time, when H_2 flow rate was 150sccm under a constant forward bias voltage of 2V at room temperature. The current decreased with hydrogen flow, and it recovered directly when the hydrogen flow was turned off. The two sensors show similar current changes with hydrogen exposure. Both adsorption and desorption times were set 5 min. The response/recovery times are additional significant factors to measure the performance of a gas sensor. The response time is defined as the time taken for the sensor to reach 90% of the saturation current from initial value while the recovery time is defined as the time taken from saturation current to reach 10% of its saturation current value after contact of the test gas with the surface of the sensor. As seen from the figure, both response and recovery times were less on Si (111) GaN sensor than those on Si (100) GaN. For example, response times taken were 3 min and 4min, while recovery times were 4.1 min and 4.5 min for Si (111) and Si (100) GaN sensors, respectively. It is interesting to note that the response and recovery time were observed to be smaller for GaN/Si(111) sample which could be explained by the quality of GaN.

© 2016 NSP
Natural Sciences Publishing Cor.

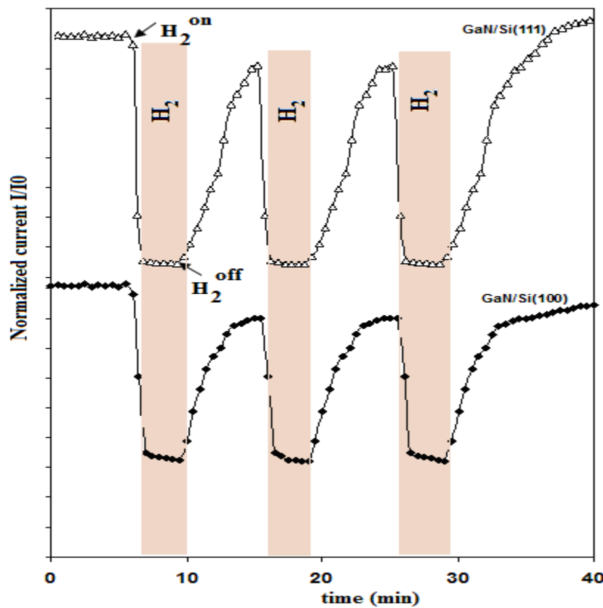

Fig. 10. Responses of the sensors toward H_2 at room temperature: (a) GaN/Si(111) and (b) GaN/Si(100).

Sensitivity is one of the important parameters that are normally used to gauge the performance of gas sensors. The sensitivity (S) was determined as the ratio (R_{gas}/R_{air}) of the resistance in hydrogen gas (R_{gas}) to that in air (R_{air}), at fixed applied voltage [33]. Fig. 11 shows the variation of sensitivity with H_2 flow rate at room temperature for the two samples recorded at 2V in forward current mode. The sensitivity increased almost linearly with hydrogen flow rate for both sensors GaN/Si (111) and GaN/Si (100) for the range up to 90 sccm and then increased exponentially. In addition, GaN on Si (111) is more sensitive to hydrogen than that on Si (100), and this may refer to that the deposition of GaN on Si (111) is better than on Si (100).

Finally, the simplest and the most commonly accepted theory of the semiconductor sensor operation mechanisms is based on the dissociation of hydrogen molecules on the metal surface and the diffusion through the metal layer and that will cause the semiconductor surface conductivity and surface potential to change. The change in surface conductivity is mainly due to variations in free electron concentration due to exchange between adsorbed species from the gas and the semiconductor surface. Thin dipole layer will be formed below the gas solid interface. This also changes the Schottky barrier height, and that will lead to change in the electrical characteristic of the device. Also a part of the reductive gas was possibly catalytically oxidized to produce water vapor and increase the measured sensor resistance. The gas sensing mechanism for the GaN sensors discussed here is different from those widely accepted and reported for GaN sensors [34-36], this is may be due to the presence of oxygen on the GaN thin films.

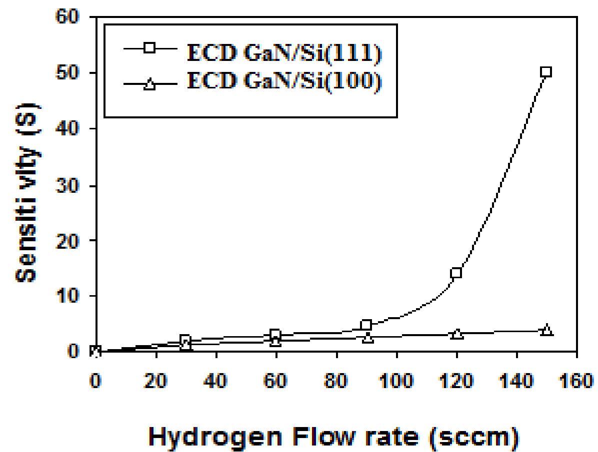

Fig. 11. Sensitivity as a function of hydrogen flow rate for MSM gas sensors of Ni/ ECD GaN on Si (111) and Si (100) at room temperature.

4 Conclusion

We have successfully fabricated and characterized Ni/GaN sensor by simple and low cost electrochemical deposition techniques. The GaN deposited films contain mixed phases of h-GaN and c-GaN with grain size in the range of 18-19 nm confirmed by XRD, PL, and Raman analyses. From SEM images, the surface morphology of the GaN films shows a network of nanoflake structures with different size. Besides, the layer was also shown to contain Ga_2O_3 in all samples. The I-V characteristic of the Schottky diode was measured before and after hydrogen gas exposure with different flow rates at room temperature. The barrier height was measured and it was found to increase with hydrogen flow rate. It was also established that the GaN on Si (111) substrate is more sensitive than the GaN on Si (100) substrate. The experimental results indicate the potential of using gallium nitride with gallium oxide face for gas sensing.

References

[1] L. Voss, B.P. Gila, S.J. Pearton, H.T. Wang, and F. Ren, J. Vac. Sci. Technol. B 23 (2005) 2373.

[2] G. Steinhoff, M. Hermann, W.J. Schaff, L.F. Eastman, M. Stutzmann, and M. Eickhoff, Appl. Phys. Lett. 83 (2003) 177.

[3] E.J. Connolly, G.M. O._Halloran, H.T.M. Pham, P.M. Sarro, and P.J. French, Sens. Actuators A Phys. 99 (2002) 25.

[4] V. Dobrokhotov, D.N. McIlroy, M.G. Norton, A. Abuzir, W.J. Yeh, I. Stevenson, R. Pouy, J. Bochenek, M. Cartwright, L. Wang, J. Dawson, M. Beaux, and C. Berven, J. Appl. Phys. 99 (2006) 104302.

[5] H. Amano, T. Tanaka, Y. Kunii, K. Kato, S.T. Kim, I. Akasaki, J Appl Phys Lett. 64 (1994) 1377-79.

© 2016 NSP
Natural Sciences Publishing Cor.

[6] S.A. Nikishin, N.N. Faleev, V. G. Antipov, S. Francoeur, L. Grave de Peralta, G.A. Seryogin, H. Temkin, T.I. Prokofyeva, M. Holtz, S.N. Chu. J Appl Phys Lett. 75 (1999) 2073-75.

[7] J. Jasinski, W. Swider, Z. Liliental-Weber, P. Visconti, K.M. Jones, M.A. Reshchikov, F. Yun, H. Morkoç, S.S. Park, K.Y. Lee. J Appl Phys Lett. 78 (2001) 2297-99.

[8] E. Nahlah, R.S. Srinivasa, S. Major, S.C. Sabharwal, K.P. Muthe. ThinSolid Films. 333(1998)9-12.

[9] J.F. Janik, R.L. Wells. Chem Mater. 8 (1996) 2708-2711.

[10] W.S. Jung, B.K. Min, Mater Lett. 58 (2004) 3058-3062.

[11] Z.H. Gu, T.Z. Fahidy. J Electrochem Soc. 146(1999)156-159.

[12] M. Izaki, T. Omi, J Electrochem Soc. 143 (1996) 53-55.

[13] J. Katayama, M. Izaki, J Appl Electrochem. 30 (2000)855-858.

[14] R.K. Roy, A.K. Pal. Materials Letters. 59(2005) 2204–2209.

[15] K. Al-Heuseen, M.R. Hashim, N.K. Ali, Mater. Lett. 64 (2010) 1604–1606.

[16] K. Al-Heuseen, M.R. Hashim. Journal of Crystal Growth 324 (2011) 274–277.

[17] C.C. Cheng, Y.Y. Tsai, K.W. Lin, H.I. Chen, W.H. Hsu, H.M. Chuang, C.Y. Chen, W.C. Liu, Semicond. Sci. Tech. 19 (2004) 778–782.

[18] J. Kim, B.P. Gila, G.Y. Chung, C.R. Abernathy, S.J. Pearton, F. Ren, Solid State Electron. 47 (2003) 1069–1073.

[19] S. Strite, H. Morkoc. J Vac Sci Technol. B10 (1992) 1237-1266.

[20] T. Detchprohm, K. Hiramatsu, K. Itoh, I. Akasaki. Jpn J Appl Phys.31 (1992) L1454-L1456.

[21] T. Barfels, H.J. Fitting, J. Jansons, I. Tale, A. Veispals, A. Czarnowski von, H.J. Wulff. Appl Surf Sci. 179(2001) 191-195.

[22] D.Y. Lee, I.S. Kim, J.S. Song. Jpn J Appl Phys 41 (2002) 4659-4662.

[23] H. Okumura, T. Takeuchi, K. Hirosawa, H. Amano, K. Hiramatsu, I. Akasaki. J Cryst Growth 128(1993) 391-396.

[24] H. Zhang, Z. Ye, B. Zhao. J Appl Phys. 87(2000) 2830-2834.

[25] L. Wang, X. Liu, Y. Zan, J. Wang, D. Lu, Z. Wang. Appl Phys Lett. 72 (1998) 109-111.

[26] G. Ramirez-Flores, H. Navarro-Contreras, A. Lastras-Martinez, R.C. Powell, J.E. Greene. Phys Rev. B50 (1994) 8433-8438.

[27] B. Deb, S. Chaudhuri, A.K. Pal. Materials Letters. 53(2002) 68– 75.

[28] S.J. Rhee, S. Kim, E.E. Reuter, S.G. Bishop, R.J. Molnar. Appl Phys Lett.73 (1998) 2636-2638.

[29] Jian Zi, Guanghong Wei, Kaiming Zhang, Xide Xie. J Phys Condensed Matter 8 (1996) 6329-6336.

[30] Y.M. Wong, W.P. Kang, J.L. Davidson, A. Wisitsora-At, K.L. Soh Sensors and Actuators B: chemical 93(1) (2003) 327-332.

[31] V.L. Rideout, Solid-State Electon. **18** (1975)541- 545.

[32] L.S. Chuah, Z. Hassan, H. Abu Hassan, N.M. Ahmed. Journal of Alloys and Compounds 481 (2009) L15–L19.

[33] H.I. Chan, Y.I. Chou, C.Y. Chu, Sensors and Actuators B: chemical. 85 (2002) 10.

[34] S. N. Das and A. K. Pal J. Phys. D: Appl. Phys. **40** (2007) 7291–7297.

[35] N.K. Ali, M.R. Hashim, A. Abdul Aziz. Solid-State Electronics 52 (2008) 1071–1074.

[36] Kang-San Kim, Gwiy-Sang Chung. Sensors and Actuators B. 160 (2011) 1232– 1236.

© 2016 NSP
Natural Sciences Publishing Cor.